

RePerformer: Immersive Human-centric Volumetric Videos from Playback to Photoreal Reperformance

Yuheng Jiang^{1,2*} Zhehao Shen^{1,2*} Chengcheng Guo¹ Yu Hong¹ Zhuo Su³
Yingliang Zhang⁴ Marc Habermann^{5†} Lan Xu^{1†}

¹ShanghaiTech University ²NeuDim ³ByteDance ⁴DGene
⁵Max Planck Institute for Informatics, Saarland Informatics Campus



Figure 1. We introduce **RePerformer**, a Gaussian-based approach for robust, high-fidelity volumetric video playback and realistic re-performance of general dynamic scenes. (Left: Sequential bass performances. Right: Synchronized violin players.)

Abstract

Human-centric volumetric videos offer immersive free-viewpoint experiences, yet existing methods focus either on replaying general dynamic scenes or animating human avatars, limiting their ability to re-perform general dynamic scenes. In this paper, we present **RePerformer**, a novel Gaussian-based representation that unifies playback and re-performance for high-fidelity human-centric volumetric videos. Specifically, we hierarchically disentangle the dynamic scenes into motion Gaussians and appearance Gaussians which are associated in the canonical space. We further employ a Morton-based parameterization to efficiently encode the appearance Gaussians into 2D position and attribute maps. For enhanced generalization, we adopt 2D CNNs to map position maps to attribute maps, which can be assembled into appearance Gaussians for high-fidelity rendering of the dynamic scenes. For re-performance, we develop a semantic-aware alignment module and apply deformation transfer on motion Gaussians, enabling photo-

real rendering under novel motions. Extensive experiments validate the robustness and effectiveness of **RePerformer**, setting a new benchmark for playback-then-reperformance paradigm in human-centric volumetric videos. Project page: <https://moqiyinlun.github.io/Reperformer/>.

1. Introduction

As the boundary between digital and real worlds continues to blur, human-centric volumetric videos represent a significant advancement in visual media, allowing users to control the virtual camera view freely. This facilitates interactive exploration and various immersive applications in telepresence, education, and entertainment.

By far, the high-end solutions for volumetric videos utilize dense multi-view videos to faithfully record the dynamic scenes. Within this domain, we observe that there are mainly two complementary workhorses for producing such human-centric volumetric videos, dubbed “*replay volumetric videos*” and “*animate volumetric videos*” for short. The former playback setting [7, 27, 73] merely reconstructs

*Equal Contribution. † Corresponding authors.

and replays the dynamic scenes. In contrast, the latter animatable setting [17, 36, 52, 74] can “reperform” the volumetric videos under novel motions unseen during recording. Both sides of research have witnessed significant changes in the underlying 3D representations, from early textured meshes [3, 8, 29], to NeRFs [24, 85], and to the very recent 3DGS [5, 30, 35]. Currently, in the playback setting, the Gaussian-based advances [27, 40] achieve high-fidelity rendering even for complex scenes like cooking or piano playing. Yet, such playback methods inherently lack the generalization ability to new motions. On the other hand, the animatable advances [5, 35, 90] mainly focus on human-only scenes (known as human avatars), heavily relying on human skeletons or parametric models like SMPL [44]. They also emphasize the generation ability to arbitrary novel motions and hence require extensive motion sequences for training.

In this paper, we explore a novel direction for human-centric volumetric video, at the intersection of the above traditional playback and animatable settings. Given a dynamic sequence with dense footage, our goal is not only deliver accurate free-view playback but also to realistically re-perform the dynamic scene under similar yet novel motions. Such a novel playback-then-reperformance setting is highly valuable with broad applications. For example, one can transfer a professional violinist’s motion to an unskilled actor in film production, resulting in realistic performances and reduced actor training costs. However, it remains challenging methodologically. Ideally, it requires animatable ability for general non-rigid scenes only given limited motion examples from a dynamic sequence, let alone maintaining photo-realism for, both, playback and re-performance.

To this end, we introduce *RePerformer*, a novel 3DGS-based approach for generating human-centric volumetric videos from dense multi-view inputs. In stark contrast to prior works, it provides realistic playback and can vividly reperform the non-rigid scenes driven by similar yet unseen motions (see Fig. 1). At the core of our RePerformer is a nuanced and hierarchical disentanglement of a dynamic Gaussian representation. We disentangle the general non-rigid scene into compact motion Gaussians and dense appearance Gaussians, akin to the Embedded deformation (ED) graph and mesh tracking [34, 70]. We further disentangle the dense appearance Gaussians into structured position maps and Gaussian attribute maps, which are associated with generalizable neural networks.

More specifically, it is a trilogy in our RePerformer. Given dense multi-view videos, **for the first tracking stage**, we disentangle motion and appearance Gaussians to provide topology-consistent tracking of the non-rigid scene. Note that both the compact motion and dense appearance Gaussians are initialized in the canonical frame and linked via nearest-neighbor search. We optimize only the positions and rotations of motion Gaussians, using them to

warp the dense Gaussians into each frame. Since the appearance Gaussians are topology-consistent, we disentangle them into 3D positions and other attributes, which are repacked into 2D position/attribute maps using a Morton-based parameterization [49] to preserve the spatial adjacency. **For the second training stage**, we perform self-supervised learning on the captured multi-view videos to learn a generalizable mapping from position maps to attribute maps. We adopt the U-Net architecture [59] with attention layers to enhance global coherence. Once trained, given the underlying motion Gaussians, we can obtain the dense position maps through non-rigid warping and then infer the corresponding attribute maps. Both maps are assembled into dense appearance Gaussians for photo-real rendering of the dynamic scene. **For further re-performance**, for new performer with novel motions, we adopt a semantic-aware alignment module to associate the motion Gaussians of the new performer with the appearance Gaussians of the original one. We then extend the deformation transfer scheme [69] into motion Gaussians, to achieve photo-real rendering under the new motions. To summarize, our main contributions include:

- We identify a new playback-then-reperformance setting for the human-centric volumetric videos.
- We present a Gaussian-based solution to achieve high-fidelity rendering of general dynamic scenes, for both playback and re-performance.
- We propose a hierarchical disentanglement scheme and a Morton-based parameterization for learning generalizable dynamic Gaussians.
- We design a semantic-aware motion transfer module to facilitate faithful re-performance across sequences.

2. Related Work

Non-rigid Reconstruction. In the field of Non-rigid registration and reconstruction, numerous methods [2, 12, 71, 72, 75, 82] have been proposed to address this challenging problem. Sumner *et al.* [70] introduces the classical embedded deformation graph for aligning two meshes, while SoG [66] utilizes a Gaussian model to represent human movement. HighQualityFVV [7] utilizes tracked mesh sequences with texture video to capture detailed human performance. Building on the pioneering work DynamicFusion [51], a series of approaches [8, 9, 25, 63, 64, 67, 68] extend this technique to handle challenging scenarios. Recent neural advances [48], bypass explicit reconstruction to conduct volume rendering at photo-realism. Based on it, dynamic NeRF variants [54, 73, 79] maintain a canonical space and leverage the photometric differences to learn the deformation. With advancements such as hash tables [50] and tensor decomposition [4], several methods [23, 26, 65, 85] significantly accelerate the training and rendering speed in the dynamic setting. However, rendering quality remains

limited. The emergence of 3D Gaussian Splatting [30] marks a significant return to explicit modeling paradigms, with dynamic variants [10, 13, 15, 22, 32, 37, 42, 45] advancing the field by tackling 4D scene reconstruction under complex scenarios. HiFi4G [28] use mesh deformation to initialize Gaussians, while DualGS [27] employs joint Gaussians for motion capture and skin Gaussians for appearance details. Although these playback-only techniques achieve high-fidelity rendering in complex scenarios like violin playing, they struggle to generalize to novel motions.

Animatable Avatar. Over the past decade, researchers have made significant progress in developing expressive and animatable 3D human avatars. Early approaches focused on mesh-based methods [1, 3, 16, 19, 62, 80, 81, 83] that utilize motion-controllable template mesh with UV space features to model human geometry and appearance. In recent years, research has increasingly shifted towards hybrid representations [18, 89] based on implicit models. ARAH [77] utilizes the SDF to model human surfaces. TAVA [36] and X-avatar [61] learn the skinning weight via Snarf [6]. DDC [17] employs differentiable rendering to learn the deformation and dynamic texture maps, while deliffas [31] enables fast light field synthesis as a follow-up work. AvatarReX [88] defines a set of local radiance fields to represent dynamic details of human appearance. Artemis [46] leverage plenotree [84] to represent animal appearances. Recent advancements in Gaussian-based representations spark a new era in animatable 3D avatars, leading to the development of innovative techniques [5, 35, 39, 53, 55, 58, 86, 87, 90]. A bunch of studies [21, 33, 56] employ linear blend skinning (LBS) to model human motions and reconstruct a 3DGS-based animatable avatar from videos. ASH [53] and GaussianAvatar [20] parameterize the 3D character on a 2D UV map while animatableGaussians [39] relies on the front and back maps to predict Gaussian attributes using 2D CNNs. However, most existing methods focus on human-only scenarios and inherently lack the ability to handle general human-object interactions. In contrast, RePerformer utilizes the Morton-based parameterization and 2D CNNs to learn the attributes of appearance Gaussians, enabling re-performance in complex human-object interactions.

3. Method

Given multi-view human performance videos (up to 81 views), our goal is to generate human-centric volumetric videos that not only deliver high-fidelity playback but also enable vivid re-performance of non-rigid scenes under similar yet unseen motions. The methodology is visually summarized in Fig. 2. Our approach begins by disentangling motion/appearance Gaussians and repacking the attributes of the appearance Gaussians into 2D maps using a Morton-based 2D parameterization. For network train-

ing, we adopt the U-Net architecture to learn a generalizable mapping from the position maps to the attribute maps. For re-performance, we adopt a semantic-aware alignment module to associate the motion Gaussians of a new performer with the original appearance Gaussians, enabling seamless transfer and photorealistic rendering.

3.1. Motion Tracking and 3D-to-2D Mapping

Tracking via Motion Gaussians. Inspired by Dynamic 3D Gaussians [45] and SoG [66], we utilize a sparse set of 3D Gaussians, denoted as Motion Gaussians, to encapsulate the underlying non-rigid motions \mathcal{M} . To effectively capture the overall movement of non-rigid scenes with minimal redundancy, we initialize approximately 50,000 Gaussian kernels in the canonical frame c using a uniform random distribution. To address the issue of insufficient geometric representation in skinny Gaussians, we enforce isotropic and size constraints, resulting in the following initialization loss:

$$E_{\text{init}} = \lambda_{\text{iso}} E_{\text{iso}} + \lambda_{\text{size}} E_{\text{size}} + E_{\text{color}}, \quad (1)$$

Please refer to DualGS [27] for detailed definitions of E_{iso} , E_{size} . For subsequent frames t , we fix spherical harmonics (SH), scaling, and opacity, using differentiable rasterization combined with a local as-rigid-as-possible constraint $E_{\text{arap}}(\mathcal{G}_{t-1}^m, \mathcal{G}_t^m)$ to achieve coherent Gaussian movement by optimizing both position p and rotation q :

$$E_{\text{arap}} = \sum_i \sum_{k \in \mathcal{N}(i)} w(p_{i,c}^m, p_{k,c}^m) \|R(q_{i,t}^m * q_{i,t-1}^{m-1}) (p_{k,t-1}^m - p_{i,t-1}^m) - (p_{k,t}^m - p_{i,t}^m)\|_2^2, \quad (2)$$

where m denotes the motion Gaussians, $\mathcal{G}_{t-1}^m, \mathcal{G}_t^m$ are adjacent frame Gaussians, k indicates the nearest 4 neighbors \mathcal{N} of the i Gaussian in the canonical frame. $R(\cdot)$ converts quaternion back into a rotation matrix and $w(p_i, p_j) = \exp(-\|p_i - p_j\|_2^2 / l^2)$ defines the weighting function.

Appearance Gaussians. Different from sparse Motion Gaussians that provide non-rigid motions, we also utilize dense 3D Gaussians ($\sim 200,000$) to serve as the splatting source of final appearance rendering, denoted as appearance Gaussians \mathcal{T} . For initialization of personalized appearance Gaussians, recent studies [39, 60] typically impose strong regularization that tightly constrains Gaussians to the mesh surface, representing them in the 2D UV space as input for powerful CNNs. However, these constraints heavily compromise rendering quality. In contrast, we train our personalized appearance Gaussians in the canonical frame without additional constraints to preserve high-fidelity details.

Once trained, given an arbitrary frame t with corresponding motion Gaussians position $p_{k,t}^m$ and rotation $q_{k,t}^m$, we identify the nearest 4 neighbors in the canonical frame c between the dense appearance Gaussians' position $p_{i,c}^{\mathcal{T}}$ and

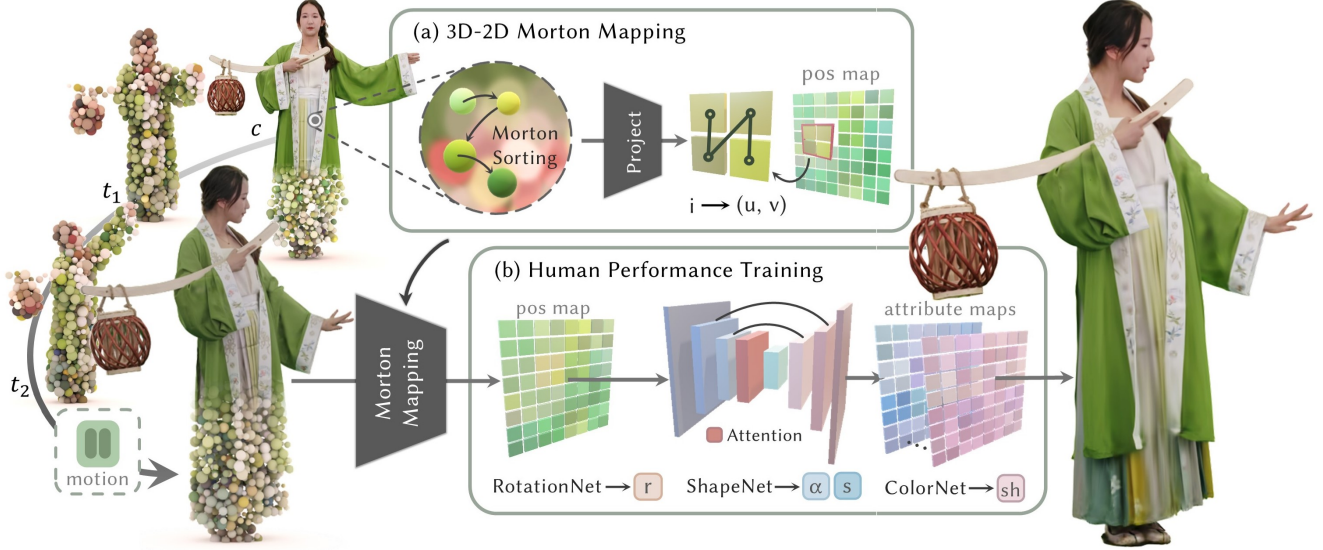


Figure 2. **Overview of RePerformer.** Our method disentangles compact motion Gaussians and dense appearance Gaussians, repacking the appearance Gaussians positions into 2D maps for network regression. (a) We use Morton parameterization to project the canonical appearance Gaussians onto UV space, forming a consistent $i \rightarrow (u, v)$ mapping. (b) RePerformer feeds the 2D position map after Morton-based parameterization into three power 2D CNNs with a self-attention layer to regress the corresponding attribute maps.

the sparse motion Gaussians’ position $p_{k,c}^m$. We then warp the dense appearance Gaussians \mathcal{G}_c^T to the target frame denoted as $\mathcal{G}_t^T = f(\mathcal{G}_c^T, \mathcal{G}_t^m)$:

$$\begin{aligned}
 p_{i,t}^T &= \sum_{k \in \mathcal{N}(p_{i,c}^T)} w(p_{i,c}^T, p_{k,c}^m) (R(\Delta q_{k,t}^m) p_{i,c}^T + \Delta p_{k,t}^m), \\
 q_{i,t}^T &= \text{slerp}_{k \in \mathcal{N}(p_{i,c}^T)} (w(p_{i,c}^T, p_{k,c}^m), \Delta q_{k,t}^m),
 \end{aligned} \tag{3}$$

Δ denotes the relative transformation with respect to the canonical frame. We use Slerp to interpolate the rotation.

Morton-based 3D-to-2D Mapping. The UV atlas of SMPL is inadequate for representing human-object scenarios. To address this, we introduce a new parameterization \mathcal{P} to project the warped appearance Gaussians onto a 2D plane as CNN input, while maintaining strong local pixel-level consistency. We first quantize the personalized appearance Gaussians’ positions and apply Morton sorting [49] to establish a Morton order, interleaving the binary representations of spatial coordinates to preserve its 3D spatial continuity. Each Gaussian i is then assigned a (u, v) coordinate based on this 2D Morton order, forming an $i \rightarrow (u, v)$ mapping, that preserves the adjacency of spatially proximate Gaussians in UV space and remains consistent across all frames. Using this mapping, we can project the personalized appearance Gaussians warped using motion Gaussians, to form the 2D position map for each frame, where (u, v) coordinates store the corresponding Gaussian positions.

3.2. Human Performance Training

Unlike DualGS, which overfits appearance Gaussians via gradient descent, we leverage efficient, well-established

2D convolutional architectures to regress the corresponding Gaussian attributes from the 2D position map, enhancing generalization capability. Considering the varying attribute distributions, we adopt U-Net [59] to learn motion-aware attribute maps, including a Rotation Net for rotation, a Shape Net for opacity and scaling, and a Color Net for the corresponding SH parameters. All attributes 2D maps are then combined with the position map and assembled to form the raw Gaussian representation \mathcal{G} .

However, Morton ordering only preserves local spatial consistency to some extent, leading that two spatially close Gaussian kernels may still be assigned to distant UV coordinates, complicating effective learning for the U-Net. To address this, we deploy a self-attention layer before the final U-Net downsampling step to capture global spatial consistency, complementing the Morton map and further improving the generalization.

Training Details. We first use background matting [41] to extract foreground masks. For motion tracking, we adopt a per-frame training strategy, achieving convergence within 20 seconds for 4,000 iterations across 20 viewpoints. For Morton mapping, We use a $(512, 512, 3)$ resolution map to store the warped appearance Gaussians positions, filling invalid UV coordinates with zeros. In the unprojection stage, we extract only valid UV coordinates for attribute maps, assembling the correct Gaussians for subsequent rasterization. For each iteration, we randomly sample a frame and a camera viewpoint, generating the corresponding position map to train three specialized U-Nets. This design improves PSNR by 0.25 dB on the DualGS dataset compared to using a single network to regress all attributes. Before the main training phase, we introduce an additional pre-training stage to

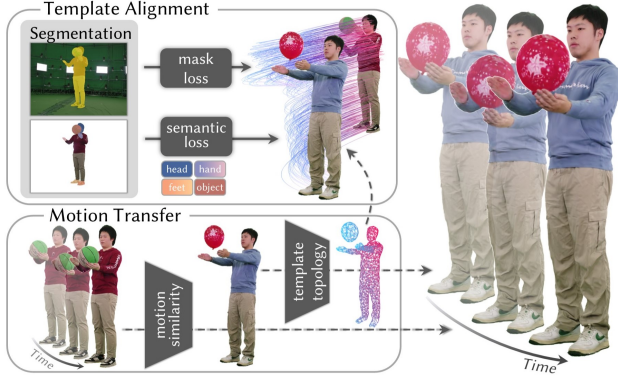


Figure 3. The re-performance pipeline consists of two components: template alignment and motion transfer.

warm up the parameters of the three networks. In this pre-training stage, we supervise the U-Net by the warped appearance Gaussians as pseudo ground truth, \mathcal{G}' . This stage optimizes the \mathcal{L}_2 loss between the pseudo ground truth and the inferred Gaussian attributes:

$$E_{\text{pre}} = \mathcal{L}_2(\mathcal{G}, \mathcal{G}'), \quad (4)$$

In the main training stage, we assemble the U-Net output attribute maps into Gaussians for rasterization, and supervise using \mathcal{L}_1 photometric loss and a D-SSIM term:

$$E_{\text{train}} = (1 - \lambda_{\text{color}}) \mathcal{L}_1 + \lambda_{\text{color}} \mathcal{L}_{\text{D-SSIM}}, \quad (5)$$

We use the Adam optimizer to train the U-Net. In the warm-up stage, we train over 2,000 iterations, with the learning rate linearly decreasing from 1 to 0.1. The main training stage consists of 180,000 iterations. The learning rates for the Rotation Net, Shape Net, and Color Net are initially set to 5×10^{-5} , 5×10^{-4} , 1×10^{-4} , respectively, and linearly decay to one-twentieth of their initial values over the training. The hyperparameters are set to $l = 0.001$, $\lambda_{\text{iso}} = 0.004$, $\lambda_{\text{size}} = 1$, $\lambda_{\text{color}} = 0.2$.

3.3. Reperformance

Popular parametric model-driven methods struggle with complex human-object interaction scenarios. As shown in Fig. 3, to handle more generalized cases, we propose a semantic-aware motion transfer module based on the motion Gaussian proxy, leveraging the U-Net generalization capability for re-performance. For the sequence s to be re-performed, we denote its appearance Gaussians in canonical space as \mathcal{G}_c^s with positions and rotations $\mathbf{p}_{i,c}^s, \mathbf{q}_{i,c}^s$. Similarly, the canonical positions and rotations of the motion Gaussians from the driving sequence r are represented as $\mathbf{p}_{i,c}^r, \mathbf{q}_{i,c}^r$, with the motion at frame t specified by $\mathbf{p}_{i,t}^r, \mathbf{q}_{i,t}^r$. Our objective is to recover transformed motions $\mathbf{p}_{i,t}^{s'}, \mathbf{q}_{i,t}^{s'}$ for the appearance Gaussians $\mathcal{G}_t^{s'}$ to be re-performed. As shown in Fig. 3, the motion transfer pipeline includes canonical alignment and motion optimization.

Alignment. Pioneering work [69] requires users to manually specify corresponding triangle faces between the source mesh and target mesh, indicating that the target triangle with index i should deform like the source triangle with index j . However, this approach is infeasible for larger, more complex Gaussian point clouds. To address this, we design a semantic-aware supervision method to establish correspondences between $\mathbf{p}_{i,c}^s$ and $\mathbf{p}_{i,c}^r$. Inspired by LanguageSAM [47], we use text prompts (e.g., right hand) and leverage GroundingDINO [43] to generate corresponding bounding boxes, which are then processed by SAM2 [57] to produce semantic masks. Following Semantic Gaussians [14], we unproject and fuse the 2D consistent semantic masks onto 3D Gaussians, assigning a semantic label to each Gaussian primitive. To establish correspondences, we perform k-means clustering on the Gaussian positions with identical labels for, both, appearance Gaussians to be re-performed and motion Gaussians for driving, respectively. We then optimize the cluster centroids to achieve a coarse alignment of Gaussian position with matching labels. The semantic alignment loss is defined as:

$$E_{\text{sem}} = \sum_{i \in \mathcal{L}} \left\| \mathbf{d}_i^{s'} - \text{sg}[\mathbf{d}_i^r] \right\|_2^2, \quad (6)$$

where \mathcal{L} is the set of semantic labels, including head, hands, feet, and objects (e.g., balloon). $\mathbf{d}_i^{s'}$ and \mathbf{d}_i^r are the centroids of the optimized source Gaussians and target for label i . sg stands for the stop-gradient operator. The overall alignment loss is defined as:

$$E_{\text{align}} = \left\| \hat{\mathcal{M}} - \mathcal{M}_r \right\|_1 + \lambda_{\text{sem}} E_{\text{sem}} + \lambda_1 E_{\text{arap}}(\mathcal{G}_c^s, \mathcal{G}_c^{s'}), \quad (7)$$

where $\hat{\mathcal{M}}$ is the alpha channel obtained from rendering the Gaussian $\mathcal{G}_c^{s'}$, and \mathcal{M}_r is the ground truth mask. The mask loss and semantic loss ensure silhouette alignment, while the arap loss preserves the topology of the appearance Gaussians to be re-performed.

Motion Transfer. To transfer the motion Gaussians deformations while preserving the topology of the appearance Gaussians to be re-performed, we optimize the position and rotation of the appearance Gaussians $\mathcal{G}_t^{s'}$ under the novel motion of \mathcal{G}_t^r . The optimization objective is defined as:

$$E_{\text{re}} = \mathcal{L}_2(\mathcal{G}_t^{s'}, f(\mathcal{G}_c^{s'}, \mathcal{G}_t^r)) + \lambda_2 E_{\text{arap}}(\mathcal{G}_c^s, \mathcal{G}_t^{s'}). \quad (8)$$

where the first term minimizes the difference between the source motion is similar to the driven motion, and the second term enforces the as-rigid-as-possible constraint to maintain the original topology of the appearance Gaussians. The optimized $\mathbf{p}_{i,t}^{s'}$ forms a new position map, retaining the same Morton order, which is then fed into the trained U-Net to recover the final re-performed Gaussians. Note that the hyperparameters are $l = 0.001$, $\lambda_{\text{sem}} = 0.001$, $\lambda_1 = 0.01$, $\lambda_2 = 0.2$.



Figure 4. Gallery of our results. RePerformer delivers high-fidelity rendering of human performance in challenging motions and achieves vivid re-performance across various complex human-object scenarios.

4. Experimental Results

4.1. Comparison

Qualitative Evaluation. We compare our RePerformer against SOTA dynamic rendering methods, including NeuS2 [78], Spacetime Gaussian [37], V^3 [76] and DualGS [27], using the DualGS dataset. As shown in Fig. 5, NeuS2 produces blurry results, while Spacetime Gaussian and V^3 , which sacrifices high-order SH for faster training, suffer from oversmoothing and a lack of rich details. Although DualGS achieves high-quality rendering, its per-frame optimization approach is computationally intensive. Yet, such methods are limited to playback and inherently lack the ability to generalize to new motions.

To validate generalization capability, we note that ex-

isting methods cannot effectively handle re-performance in general human-object interaction scenarios. Thus, we select control-point-driven and template-free modeling approaches, training them in a multi-view setting to evaluate their rendering quality on novel views and motions. As depicted in Fig. 6, Articulated-Point-NeRF [74], which relies heavily on TiNeuVox [11], exhibits significant artifacts when training on complex, long sequences. Similarly, TAVA [36] faces difficulties with challenging motions, failing to capture fine appearance details, while SC-GS [22] achieves reasonable rendering quality for novel views but suffers severe degradation in appearance quality with novel poses. In contrast, RePerformer leverages Morton-based parameterization and a U-Net with self-attention to ensure 2D consistency, enabling high-fidelity rendering for, both,



Figure 5. Qualitative comparison with SOTA playback-only methods on novel view synthesis on DualGS dataset.

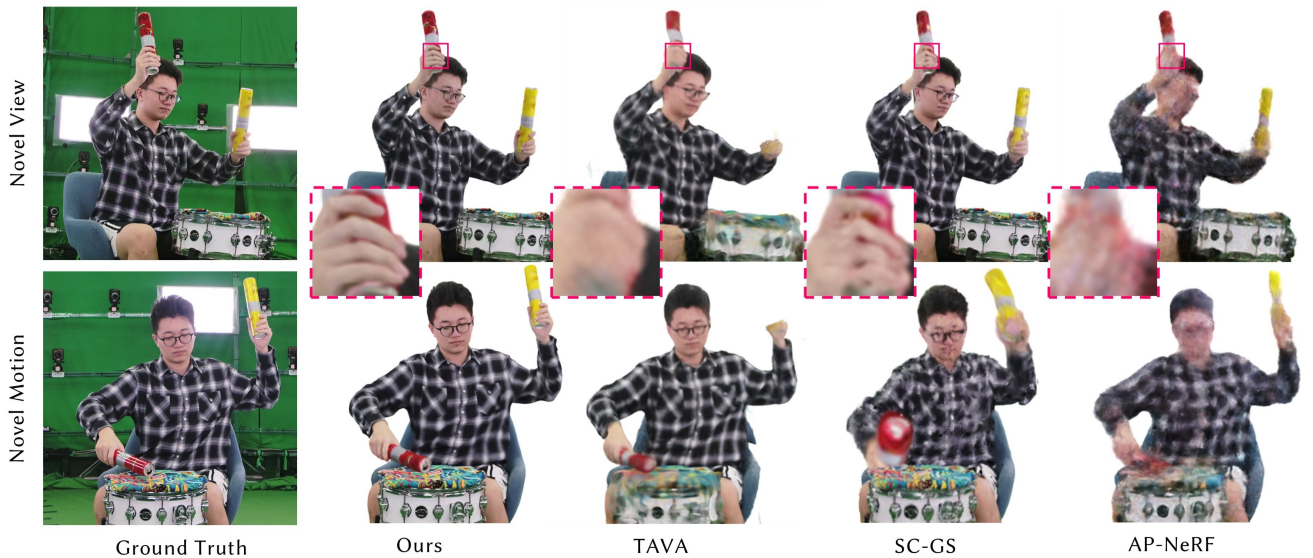


Figure 6. Qualitative comparison with AP-NeRF [74], TAVA [36] and SC-GS [22] on both training motion and novel motion synthesis.

novel views and novel motions. As illustrated in Fig. 4, our method effectively addresses the dual challenges of playback and re-performance across various complex human-object scenarios.

Quantitative Comparison. We select three 500-frame sequences from the DualGS dataset and evaluate performance across 8 test views using metrics such as PSNR, SSIM, LPIPS, and training time. As shown in Tab. 1, RePerformer ranks second, slightly behind per-frame optimized DualGS, with significantly reduced training time thanks to 2D CNNs’ generalization ability.

To assess generalization, we use a 3,000-frame sequence, training on frames 1 to 2,500 and testing on frames 2,500 to 3,000. As illustrated in Tab. 2, RePerformer outperforms all other methods across multiple metrics, demonstrating superior rendering quality and strong generalization capability.

Method	PSNR \uparrow	SSIM \uparrow	LPIPS \downarrow	Training Time(Min / frame) \downarrow
NeuS2 [78]	29.589	0.967	0.0561	3.23
Spacetime Gaussian [37]	31.691	0.981	0.0289	2.24
DualGS [27]	35.506	0.990	0.0193	12.22
V^3 [76]	33.821	0.984	0.0167	1.86
Ours	34.571	0.986	0.0229	1.68

Table 1. Quantitative comparison of novel view rendering. Green and yellow cell colors indicate the best and the second-best results.

4.2. Ablation Study

Training Strategy. We conduct a qualitative ablation study on 500 frames, comparing different 3D-to-2D parameterization methods: Morton, y-axis order, and random mapping, to evaluate their effectiveness. As shown in Fig. 7, Morton parameterization outperforms both y-axis and random mappings in convergence speed and rendering quality. The

Methods	Novel View			Novel Motion		
	PSNR \uparrow	SSIM \uparrow	LPIPS \downarrow	PSNR \uparrow	SSIM \uparrow	LPIPS \downarrow
AP-NeRF [74]	28.26	0.939	0.0768	26.85	0.944	0.0519
TAVA [36]	21.57	0.906	0.1292	21.34	0.905	0.1301
SC-GS [22]	30.63	0.971	0.0319	19.18	0.907	0.0821
Ours	32.09	0.979	0.0310	30.06	0.976	0.0277

Table 2. Quantitative comparison with template-free modeling approaches in both novel views and motions.

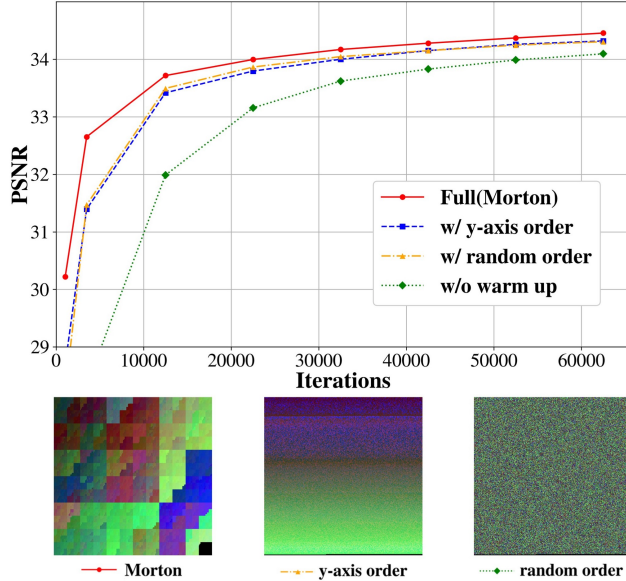


Figure 7. Qualitative ablation study on training strategy. Our full pipeline achieves the fastest convergence and highest quality.

bottom images show position maps normalized to the RGB color space, demonstrating Morton mapping that preserves local consistency in UV space. Additionally, skipping the warm-up stage leads to slower convergence during training.

Alignment. We assess the impact of each term in Eq. 7. As depicted in Fig. 8, excluding E_{sem} leads to unnatural artifacts, while omitting E_{arap} results in severe noise. In contrast, our complete method successfully aligns the source with the target, while maintaining topological consistency.

Motion Transfer. We analyze the influence of E_{arap} in Eq. 8, examining the trade-off between motion similarity and topological consistency. As shown in Fig. 9, excluding E_{arap} causes unrealistic deformations and artifacts in the appearance Gaussians, even after U-Net processing. Including the E_{arap} term significantly alleviates these issues, leading to more realistic rendering for novel motions.

5. Limitations

Despite RePerformer achieving high-fidelity rendering for novel views and motions, it has several limitations. First, although our motion Gaussians effectively capture dynamics in non-rigid scenes, the process remains time-consuming (20 seconds per frame), limiting real-time applications. Accelerating this step is a promising direction for future re-

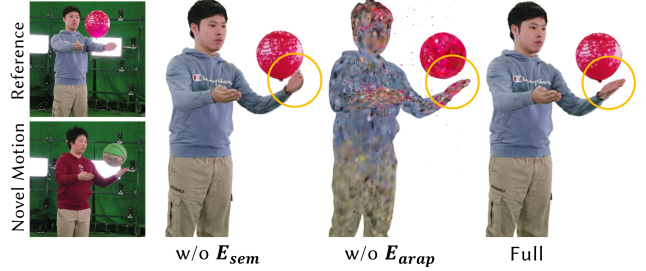


Figure 8. Qualitative ablation study on alignment component.



Figure 9. Qualitative ablation study on motion transfer.

search. Second, RePerformer struggles to generalize across arbitrary motions. The quality of re-performance relies heavily on having similar interaction types, collecting large-scale datasets could enhance generalization. Finally, we utilized only one self-attention layer due to GPU memory constraints. Using additional layers could further enhance generalization.

6. Conclusion

We have introduced a Gaussian-based approach that not only delivers high-fidelity playback but also enables vivid re-performance of general non-rigid scenes. Our approach disentangles general non-rigid scenes into compact motion Gaussians and dense appearance Gaussians, and employs a Morton-based parameterization to repack the appearance Gaussians into 2D position maps. We utilize the U-Net architecture to regress the corresponding attribute maps of the position maps, which are assembled into appearance Gaussians for photorealistic rendering. We also introduce a semantic-aware alignment module that transfers motion Gaussians from a new performer to the original scene for re-performance. Comprehensive experiments demonstrate that RePerformer outperforms state-of-the-art methods in rendering quality and generalization capability. With the unique and faithful playback and re-performance ability, we believe our approach can serve as a solid step towards immersive human-centric volumetric videos.

Acknowledgements. This work was supported by the National Key R&D Program of China (2022YFF0902301), Shanghai Local College Capacity Building Program (22010502800), and Shanghai Frontiers Science Center of Human-centered AI (ShangHAI).

References

- [1] Timur Bagautdinov, Chenglei Wu, Tomas Simon, Fabian Prada, Takaaki Shiratori, Shih-En Wei, Weipeng Xu, Yaser Sheikh, and Jason Saragih. Driving-signal aware full-body avatars. *ACM Transactions on Graphics (TOG)*, 40(4):1–17, 2021. 3
- [2] Ang Cao and Justin Johnson. Hexplane: A fast representation for dynamic scenes. In *Proceedings of the IEEE/CVF Conference on Computer Vision and Pattern Recognition*, pages 130–141, 2023. 2
- [3] Dan Casas, Marco Volino, John Collomosse, and Adrian Hilton. 4d video textures for interactive character appearance. In *Computer Graphics Forum*, pages 371–380. Wiley Online Library, 2014. 2, 3
- [4] Anpei Chen, Zexiang Xu, Andreas Geiger, Jingyi Yu, and Hao Su. Tensorf: Tensorial radiance fields. In *European Conference on Computer Vision*, pages 333–350. Springer, 2022. 2
- [5] Jianchun Chen, Jian Wang, Yinda Zhang, Rohit Pandey, Thabo Beeler, Marc Habermann, and Christian Theobalt. Egoavatar: Egocentric view-driven and photorealistic full-body avatars. In *SIGGRAPH Asia 2024 Conference Papers*, pages 1–11, 2024. 2, 3
- [6] Xu Chen, Yufeng Zheng, Michael J Black, Otmar Hilliges, and Andreas Geiger. Snarf: Differentiable forward skinning for animating non-rigid neural implicit shapes. In *Proceedings of the IEEE/CVF International Conference on Computer Vision*, pages 11594–11604, 2021. 3
- [7] Alvaro Collet, Ming Chuang, Pat Sweeney, Don Gillett, Dennis Evseev, David Calabrese, Hugues Hoppe, Adam Kirk, and Steve Sullivan. High-quality streamable free-viewpoint video. *ACM Transactions on Graphics (TOG)*, 34(4):69, 2015. 1, 2
- [8] Mingsong Dou, Sameh Khamis, Yury Degtyarev, Philip Davidson, Sean Ryan Fanello, Adarsh Kowdle, Sergio Orts Escolano, Christoph Rhemann, David Kim, Jonathan Taylor, Pushmeet Kohli, Vladimir Tankovich, and Shahram Izadi. Fusion4d: real-time performance capture of challenging scenes. *ACM Trans. Graph.*, 35(4), 2016. 2
- [9] Mingsong Dou, Philip Davidson, Sean Ryan Fanello, Sameh Khamis, Adarsh Kowdle, Christoph Rhemann, Vladimir Tankovich, and Shahram Izadi. Motion2fusion: Real-time volumetric performance capture. *ACM Trans. Graph.*, 36(6): 246:1–246:16, 2017. 2
- [10] Yuanxing Duan, Fangyin Wei, Qiyu Dai, Yuhang He, Wenzheng Chen, and Baoquan Chen. 4d-rotor gaussian splatting: towards efficient novel view synthesis for dynamic scenes. In *ACM SIGGRAPH 2024 Conference Papers*, pages 1–11, 2024. 3
- [11] Jiemin Fang, Taoran Yi, Xinggang Wang, Lingxi Xie, Xiao-peng Zhang, Wenyu Liu, Matthias Nießner, and Qi Tian. Fast dynamic radiance fields with time-aware neural voxels. In *SIGGRAPH Asia 2022 Conference Papers*, 2022. 6
- [12] Sara Fridovich-Keil, Giacomo Meanti, Frederik Rahbæk Warburg, Benjamin Recht, and Angjoo Kanazawa. K-planes: Explicit radiance fields in space, time, and appearance. In *Proceedings of the IEEE/CVF Conference on Computer Vision and Pattern Recognition*, pages 12479–12488, 2023. 2
- [13] Quankai Gao, Qiangeng Xu, Zhe Cao, Ben Mildenhall, Wen-chao Ma, Le Chen, Danhang Tang, and Ulrich Neumann. Gaussianflow: Splatting gaussian dynamics for 4d content creation. *arXiv preprint arXiv:2403.12365*, 2024. 3
- [14] Jun Guo, Xiaojian Ma, Yue Fan, Huaping Liu, and Qing Li. Semantic gaussians: Open-vocabulary scene understanding with 3d gaussian splatting. *arXiv preprint arXiv:2403.15624*, 2024. 5
- [15] Zhiyang Guo, Wengang Zhou, Li Li, Min Wang, and Houqiang Li. Motion-aware 3d gaussian splatting for efficient dynamic scene reconstruction. *IEEE Transactions on Circuits and Systems for Video Technology*, 2024. 3
- [16] Marc Habermann, Weipeng Xu, Michael Zollhoefer, Gerard Pons-Moll, and Christian Theobalt. Deepcap: Monocular human performance capture using weak supervision. In *IEEE Conference on Computer Vision and Pattern Recognition (CVPR)*. IEEE, 2020. 3
- [17] Marc Habermann, Lingjie Liu, Weipeng Xu, Michael Zollhoefer, Gerard Pons-Moll, and Christian Theobalt. Real-time deep dynamic characters. *ACM Transactions on Graphics (ToG)*, 40(4):1–16, 2021. 2, 3
- [18] Marc Habermann, Lingjie Liu, Weipeng Xu, Gerard Pons-Moll, Michael Zollhoefer, and Christian Theobalt. Hdhumans: A hybrid approach for high-fidelity digital humans. *Proceedings of the ACM on Computer Graphics and Interactive Techniques*, 6(3):1–23, 2023. 3
- [19] Oshri Halimi, Tuur Stuyck, Donglai Xiang, Timur M Bagautdinov, He Wen, Ron Kimmel, Takaaki Shiratori, Chenglei Wu, Yaser Sheikh, and Fabian Prada. Pattern-based cloth registration and sparse-view animation. *ACM Trans. Graph.*, 41(6):196–1, 2022. 3
- [20] Liangxiao Hu, Hongwen Zhang, Yuxiang Zhang, Boyao Zhou, Boning Liu, Shengping Zhang, and Liqiang Nie. Gaussianavatar: Towards realistic human avatar modeling from a single video via animatable 3d gaussians. In *Proceedings of the IEEE/CVF Conference on Computer Vision and Pattern Recognition*, pages 634–644, 2024. 3
- [21] Shoukang Hu, Tao Hu, and Ziwei Liu. Gauhuman: Articulated gaussian splatting from monocular human videos. In *Proceedings of the IEEE/CVF Conference on Computer Vision and Pattern Recognition*, pages 20418–20431, 2024. 3
- [22] Yi-Hua Huang, Yang-Tian Sun, Ziyi Yang, Xiaoyang Lyu, Yan-Pei Cao, and Xiaojuan Qi. Sc-gs: Sparse-controlled gaussian splatting for editable dynamic scenes. In *Proceedings of the IEEE/CVF Conference on Computer Vision and Pattern Recognition*, pages 4220–4230, 2024. 3, 6, 7, 8
- [23] Mustafa Işık, Martin Rünz, Markos Georgopoulos, Taras Khakhulin, Jonathan Starck, Lourdes Agapito, and Matthias Nießner. Humanrf: High-fidelity neural radiance fields for humans in motion. *ACM Transactions on Graphics (TOG)*, 42(4):1–12, 2023. 2
- [24] Tianjian Jiang, Xu Chen, Jie Song, and Otmar Hilliges. Instantavatar: Learning avatars from monocular video in 60 seconds. In *Proceedings of the IEEE/CVF Conference on Computer Vision and Pattern Recognition*, pages 16922–16932, 2023. 2

- [25] Yuheng Jiang, Suyi Jiang, Guoxing Sun, Zhuo Su, Kaiwen Guo, Minye Wu, Jingyi Yu, and Lan Xu. Neuralhofusion: Neural volumetric rendering under human-object interactions. In *Proceedings of the IEEE/CVF Conference on Computer Vision and Pattern Recognition*, pages 6155–6165, 2022. 2
- [26] Yuheng Jiang, Kaixin Yao, Zhuo Su, Zhehao Shen, Haimin Luo, and Lan Xu. Instant-nvr: Instant neural volumetric rendering for human-object interactions from monocular rgbd stream. In *Proceedings of the IEEE/CVF Conference on Computer Vision and Pattern Recognition*, pages 595–605, 2023. 2
- [27] Yuheng Jiang, Zhehao Shen, Yu Hong, Chengcheng Guo, Yize Wu, Yingliang Zhang, Jingyi Yu, and Lan Xu. Robust dual gaussian splatting for immersive human-centric volumetric videos. *ACM Transactions on Graphics (TOG)*, 43(6):1–15, 2024. 1, 2, 3, 6, 7
- [28] Yuheng Jiang, Zhehao Shen, Penghao Wang, Zhuo Su, Yu Hong, Yingliang Zhang, Jingyi Yu, and Lan Xu. Hifi4g: High-fidelity human performance rendering via compact gaussian splatting. In *Proceedings of the IEEE/CVF Conference on Computer Vision and Pattern Recognition*, pages 19734–19745, 2024. 3
- [29] Hanbyul Joo, Tomas Simon, and Yaser Sheikh. Total capture: A 3d deformation model for tracking faces, hands, and bodies. In *The IEEE Conference on Computer Vision and Pattern Recognition (CVPR)*, 2018. 2
- [30] Bernhard Kerbl, Georgios Kopanas, Thomas Leimkühler, and George Drettakis. 3d gaussian splatting for real-time radiance field rendering. *ACM Transactions on Graphics (TOG)*, 42(4):1–14, 2023. 2, 3, 1
- [31] Youngjoong Kwon, Lingjie Liu, Henry Fuchs, Marc Habermann, and Christian Theobalt. Deliffas: Deformable light fields for fast avatar synthesis. *Advances in Neural Information Processing Systems*, 2023. 3
- [32] Isaac Labe, Noam Issachar, Itai Lang, and Sagie Benaim. Dgd: Dynamic 3d gaussians distillation. In *European Conference on Computer Vision*, pages 361–378. Springer, 2024. 3
- [33] Jiahui Lei, Yufu Wang, Georgios Pavlakos, Lingjie Liu, and Kostas Daniilidis. Gart: Gaussian articulated template models. In *Proceedings of the IEEE/CVF Conference on Computer Vision and Pattern Recognition*, pages 19876–19887, 2024. 3
- [34] Hao Li, Robert W Sumner, and Mark Pauly. Global correspondence optimization for non-rigid registration of depth scans. In *Computer graphics forum*, pages 1421–1430. Wiley Online Library, 2008. 2
- [35] Mengtian Li, Shengxiang Yao, Zhifeng Xie, Keyu Chen, and Yu-Gang Jiang. Gaussianbody: Clothed human reconstruction via 3d gaussian splatting. *arXiv preprint arXiv:2401.09720*, 2024. 2, 3
- [36] Ruilong Li, Julian Tanke, Minh Vo, Michael Zollhöfer, Jürgen Gall, Angjoo Kanazawa, and Christoph Lassner. Tava: Template-free animatable volumetric actors. In *European Conference on Computer Vision*, pages 419–436. Springer, 2022. 2, 3, 6, 7, 8
- [37] Zhan Li, Zhang Chen, Zhong Li, and Yi Xu. Spacetime gaussian feature splatting for real-time dynamic view synthesis. In *Proceedings of the IEEE/CVF Conference on Computer Vision and Pattern Recognition*, pages 8508–8520, 2024. 3, 6, 7
- [38] Zhe Li, Zerong Zheng, Lizhen Wang, and Yebin Liu. Animatable gaussians: Learning pose-dependent gaussian maps for high-fidelity human avatar modeling. In *Proceedings of the IEEE/CVF Conference on Computer Vision and Pattern Recognition*, pages 19711–19722, 2024. 1, 2
- [39] Zhe Li, Zerong Zheng, Lizhen Wang, and Yebin Liu. Animatable gaussians: Learning pose-dependent gaussian maps for high-fidelity human avatar modeling. In *Proceedings of the IEEE/CVF Conference on Computer Vision and Pattern Recognition (CVPR)*, 2024. 3
- [40] Yiqing Liang, Numair Khan, Zhengqin Li, Thu Nguyen-Phuoc, Douglas Lanman, James Tompkin, and Lei Xiao. Gafre: Gaussian deformation fields for real-time dynamic novel view synthesis. *arXiv preprint arXiv:2312.11458*, 2023. 2
- [41] Shanchuan Lin, Andrey Ryabtsev, Soumyadip Sengupta, Brian L Curless, Steven M Seitz, and Ira Kemelmacher-Shlizerman. Real-time high-resolution background matting. In *Proceedings of the IEEE/CVF Conference on Computer Vision and Pattern Recognition*, pages 8762–8771, 2021. 4
- [42] Youtian Lin, Zuozhuo Dai, Siyu Zhu, and Yao Yao. Gaussian-flow: 4d reconstruction with dynamic 3d gaussian particle. In *Proceedings of the IEEE/CVF Conference on Computer Vision and Pattern Recognition*, pages 21136–21145, 2024. 3
- [43] Shilong Liu, Zhaoyang Zeng, Tianhe Ren, Feng Li, Hao Zhang, Jie Yang, Qing Jiang, Chunyuan Li, Jianwei Yang, Hang Su, et al. Grounding dino: Marrying dino with grounded pre-training for open-set object detection. In *European Conference on Computer Vision*, pages 38–55. Springer, 2024. 5
- [44] Matthew Loper, Naureen Mahmood, Javier Romero, Gerard Pons-Moll, and Michael J. Black. Smpl: A skinned multi-person linear model. *ACM Trans. Graph.*, 34(6):248:1–248:16, 2015. 2, 1
- [45] Jonathon Luiten, Georgios Kopanas, Bastian Leibe, and Deva Ramanan. Dynamic 3d gaussians: Tracking by persistent dynamic view synthesis. In *3DV*, 2024. 3
- [46] Haimin Luo, Teng Xu, Yuheng Jiang, Chenglin Zhou, Qiwei Qiu, Yingliang Zhang, Wei Yang, Lan Xu, and Jingyi Yu. Artemis: Articulated neural pets with appearance and motion synthesis. *ACM Trans. Graph.*, 41(4), 2022. 3
- [47] Luca Medeiros. Lang-segment-anything. <https://github.com/luca-medeiros/lang-segment-anything>, 2024. Accessed: 2024-11-08. 5
- [48] Ben Mildenhall, Pratul P. Srinivasan, Matthew Tancik, Jonathan T. Barron, Ravi Ramamoorthi, and Ren Ng. Nerf: Representing scenes as neural radiance fields for view synthesis. In *Computer Vision – ECCV 2020*, pages 405–421. Cham, 2020. Springer International Publishing. 2
- [49] Guy M Morton. A computer oriented geodetic data base and a new technique in file sequencing. 1966. 2, 4

- [50] Thomas Müller, Alex Evans, Christoph Schied, and Alexander Keller. Instant neural graphics primitives with a multiresolution hash encoding. *ACM Trans. Graph.*, 41(4):102:1–102:15, 2022. 2
- [51] Richard A Newcombe, Dieter Fox, and Steven M Seitz. Dynamicfusion: Reconstruction and tracking of non-rigid scenes in real-time. In *Proceedings of the IEEE conference on computer vision and pattern recognition*, pages 343–352, 2015. 2
- [52] Atsuhiko Noguchi, Xiao Sun, Stephen Lin, and Tatsuya Harada. Neural articulated radiance field. In *Proceedings of the IEEE/CVF International Conference on Computer Vision*, pages 5762–5772, 2021. 2
- [53] Haokai Pang, Heming Zhu, Adam Kortylewski, Christian Theobalt, and Marc Habermann. Ash: Animatable gaussian splats for efficient and photoreal human rendering. In *Proceedings of the IEEE/CVF Conference on Computer Vision and Pattern Recognition*, pages 1165–1175, 2024. 3
- [54] Keunhong Park, Utkarsh Sinha, Jonathan T Barron, Sofien Bouaziz, Dan B Goldman, Steven M Seitz, and Ricardo Martin-Brualla. Nerfies: Deformable neural radiance fields. In *Proceedings of the IEEE/CVF International Conference on Computer Vision*, pages 5865–5874, 2021. 2
- [55] Shenhan Qian, Tobias Kirschstein, Liam Schoneveld, Davide Davoli, Simon Giebenhain, and Matthias Nießner. Gaussianavatars: Photorealistic head avatars with rigged 3d gaussians. In *Proceedings of the IEEE/CVF Conference on Computer Vision and Pattern Recognition*, pages 20299–20309, 2024. 3
- [56] Zhiyin Qian, Shaofei Wang, Marko Mihajlovic, Andreas Geiger, and Siyu Tang. 3dgs-avatar: Animatable avatars via deformable 3d gaussian splatting. In *Proceedings of the IEEE/CVF Conference on Computer Vision and Pattern Recognition*, pages 5020–5030, 2024. 3
- [57] Nikhila Ravi, Valentin Gabeur, Yuan-Ting Hu, Ronghang Hu, Chaitanya Ryali, Tengyu Ma, Haitham Khedr, Roman Rädle, Chloe Rolland, Laura Gustafson, et al. Sam 2: Segment anything in images and videos. *arXiv preprint arXiv:2408.00714*, 2024. 5
- [58] Boxiang Rong, Artur Grigorev, Wenbo Wang, Michael J Black, Bernhard Thomaszewski, Christina Tsalicoglou, and Otmar Hilliges. Gaussian garments: Reconstructing simulation-ready clothing with photorealistic appearance from multi-view video. *arXiv preprint arXiv:2409.08189*, 2024. 3
- [59] Olaf Ronneberger, Philipp Fischer, and Thomas Brox. U-net: Convolutional networks for biomedical image segmentation. In *International Conference on Medical image computing and computer-assisted intervention*, pages 234–241. Springer, 2015. 2, 4
- [60] Zhijing Shao, Duotun Wang, Qing-Yao Tian, Yao-Dong Yang, Hengyu Meng, Zeyu Cai, Bo Dong, Yu Zhang, Kang Zhang, and Zeyu Wang. Degas: Detailed expressions on full-body gaussian avatars. *arXiv preprint arXiv:2408.10588*, 2024. 3
- [61] Kaiyue Shen, Chen Guo, Manuel Kaufmann, Juan Jose Zarate, Julien Valentin, Jie Song, and Otmar Hilliges. X-avatar: Expressive human avatars. In *Proceedings of the IEEE/CVF Conference on Computer Vision and Pattern Recognition*, pages 16911–16921, 2023. 3
- [62] Aliaksandra Shysheya, Egor Zakharov, Kara-Ali Aliev, Renat Bashirov, Egor Burkov, Karim Iskakov, Aleksei Ivakhnenko, Yury Malkov, Igor Pasechnik, Dmitry Ulyanov, et al. Textured neural avatars. In *Proceedings of the IEEE/CVF Conference on Computer Vision and Pattern Recognition*, pages 2387–2397, 2019. 3
- [63] Miroslava Slavcheva, Maximilian Baust, Daniel Cremers, and Slobodan Ilic. Killingfusion: Non-rigid 3d reconstruction without correspondences. In *Proceedings of the IEEE Conference on Computer Vision and Pattern Recognition*, pages 1386–1395, 2017. 2
- [64] Miroslava Slavcheva, Maximilian Baust, and Slobodan Ilic. Sobolevfusion: 3d reconstruction of scenes undergoing free non-rigid motion. In *Proceedings of the IEEE conference on computer vision and pattern recognition*, pages 2646–2655, 2018. 2
- [65] Liangchen Song, Anpei Chen, Zhong Li, Zhang Chen, Lele Chen, Junsong Yuan, Yi Xu, and Andreas Geiger. Nerf-player: A streamable dynamic scene representation with decomposed neural radiance fields. *IEEE Transactions on Visualization and Computer Graphics*, 29(5):2732–2742, 2023. 2
- [66] Carsten Stoll, Nils Hasler, Juergen Gall, Hans-Peter Seidel, and Christian Theobalt. Fast articulated motion tracking using a sums of Gaussians body model. In *International Conference on Computer Vision (ICCV)*, 2011. 2, 3
- [67] Zhuo Su, Lan Xu, Zerong Zheng, Tao Yu, Yebin Liu, and Lu Fang. Robustfusion: Human volumetric capture with data-driven visual cues using a rgbd camera. In *Computer Vision – ECCV 2020*, pages 246–264, Cham, 2020. Springer International Publishing. 2
- [68] Zhuo Su, Lan Xu, Dawei Zhong, Zhong Li, Fan Deng, Shuxue Quan, and Lu Fang. Robustfusion: Robust volumetric performance reconstruction under human-object interactions from monocular rgbd stream. *IEEE Transactions on Pattern Analysis and Machine Intelligence*, 2022. 2
- [69] Robert W Sumner and Jovan Popović. Deformation transfer for triangle meshes. *ACM Transactions on graphics (TOG)*, 23(3):399–405, 2004. 2, 5
- [70] Robert W Sumner, Johannes Schmid, and Mark Pauly. Embedded deformation for shape manipulation. *ACM Transactions on Graphics (TOG)*, 26(3):80, 2007. 2
- [71] Guoxing Sun, Xin Chen, Yizhang Chen, Anqi Pang, Pei Lin, Yuheng Jiang, Lan Xu, Jingya Wang, and Jingyi Yu. Neural free-viewpoint performance rendering under complex human-object interactions. In *Proceedings of the 29th ACM International Conference on Multimedia*, 2021. 2
- [72] Xin Suo, Yuheng Jiang, Pei Lin, Yingliang Zhang, Minye Wu, Kaiwen Guo, and Lan Xu. Neuralhumanfvv: Real-time neural volumetric human performance rendering using rgb cameras. In *Proceedings of the IEEE/CVF Conference on Computer Vision and Pattern Recognition*, pages 6226–6237, 2021. 2
- [73] Edgar Tretschk, Ayush Tewari, Vladislav Golyanik, Michael Zollhöfer, Christoph Lassner, and Christian Theobalt. Non-rigid neural radiance fields: Reconstruction and novel view

- synthesis of a dynamic scene from monocular video. In *IEEE International Conference on Computer Vision (ICCV)*. IEEE, 2021. 1, 2
- [74] Lukas Uzolas, Elmar Eisemann, and Petr Kellnhofer. Template-free articulated neural point clouds for reposable view synthesis. *Advances in Neural Information Processing Systems*, 36, 2024. 2, 6, 7, 8
- [75] Liao Wang, Kaixin Yao, Chengcheng Guo, Zhirui Zhang, Qiang Hu, Jingyi Yu, Lan Xu, and Minye Wu. Videorf: Rendering dynamic radiance fields as 2d feature video streams. In *Proceedings of the IEEE/CVF Conference on Computer Vision and Pattern Recognition*, pages 470–481, 2024. 2
- [76] Penghao Wang, Zhirui Zhang, Liao Wang, Kaixin Yao, Siyuan Xie, Jingyi Yu, Minye Wu, and Lan Xu. V³: Viewing volumetric videos on mobiles via streamable 2d dynamic gaussians. *ACM Transactions on Graphics (TOG)*, 43(6):1–13, 2024. 6, 7
- [77] Shaofei Wang, Katja Schwarz, Andreas Geiger, and Siyu Tang. Arah: Animatable volume rendering of articulated human sdf. In *European Conference on Computer Vision*, 2022. 3
- [78] Yiming Wang, Qin Han, Marc Habermann, Kostas Daniilidis, Christian Theobalt, and Lingjie Liu. Neus2: Fast learning of neural implicit surfaces for multi-view reconstruction. In *Proceedings of the IEEE/CVF International Conference on Computer Vision*, pages 3295–3306, 2023. 6, 7
- [79] Chung-Yi Weng, Brian Curless, Pratul P. Srinivasan, Jonathan T. Barron, and Ira Kemelmacher-Shlizerman. HumanNeRF: Free-viewpoint rendering of moving people from monocular video. In *Proceedings of the IEEE/CVF Conference on Computer Vision and Pattern Recognition (CVPR)*, pages 16210–16220, 2022. 2
- [80] Donglai Xiang, Fabian Prada, Timur Bagautdinov, Weipeng Xu, Yuan Dong, He Wen, Jessica Hodgins, and Chenglei Wu. Modeling clothing as a separate layer for an animatable human avatar. *ACM Transactions on Graphics (TOG)*, 40(6):1–15, 2021. 3
- [81] Donglai Xiang, Timur Bagautdinov, Tuur Stuyck, Fabian Prada, Javier Romero, Weipeng Xu, Shunsuke Saito, Jingfan Guo, Breannan Smith, Takaaki Shiratori, Yaser Sheikh, Jessica Hodgins, and Chenglei Wu. Dressing avatars: Deep photorealistic appearance for physically simulated clothing. *ACM Trans. Graph.*, 41(6), 2022. 3
- [82] Lan Xu, Zhuo Su, Lei Han, Tao Yu, Yebin Liu, and Lu Fang. Unstructuredfusion: realtime 4d geometry and texture reconstruction using commercial rgb cameras. *IEEE transactions on pattern analysis and machine intelligence*, 42(10):2508–2522, 2019. 2
- [83] Weipeng Xu, Avishek Chatterjee, Michael Zollhöfer, Helge Rhodin, Dushyant Mehta, Hans-Peter Seidel, and Christian Theobalt. Monoperfcap: Human performance capture from monocular video. *ACM Transactions on Graphics (TOG)*, 37(2):27:1–27:15, 2018. 3
- [84] Alex Yu, Ruilong Li, Matthew Tancik, Hao Li, Ren Ng, and Angjoo Kanazawa. Plenotrees for real-time rendering of neural radiance fields. In *Proceedings of the IEEE/CVF International Conference on Computer Vision*, pages 5752–5761, 2021. 3
- [85] Fuqiang Zhao, Yuheng Jiang, Kaixin Yao, Jiakai Zhang, Liao Wang, Haizhao Dai, Yuhui Zhong, Yingliang Zhang, Minye Wu, Lan Xu, and Jingyi Yu. Human performance modeling and rendering via neural animated mesh. *ACM Trans. Graph.*, 41(6), 2022. 2
- [86] Xiaozheng Zheng, Chao Wen, Zhaohu Li, Weiyi Zhang, Zhuo Su, Xu Chang, Yang Zhao, Zheng Lv, Xiaoyuan Zhang, Yongjie Zhang, et al. Headgap: Few-shot 3d head avatar via generalizable gaussian priors. *arXiv preprint arXiv:2408.06019*, 2024. 3
- [87] Xiaozheng Zheng, Chao Wen, Zhuo Su, Zeran Xu, Zhaohu Li, Yang Zhao, and Zhou Xue. Ohta: One-shot hand avatar via data-driven implicit priors. In *Proceedings of the IEEE/CVF Conference on Computer Vision and Pattern Recognition*, pages 799–810, 2024. 3
- [88] Zerong Zheng, Xiaochen Zhao, Hongwen Zhang, Boning Liu, and Yebin Liu. Avatarrex: Real-time expressive full-body avatars. *ACM Transactions on Graphics (TOG)*, 42(4), 2023. 3
- [89] Heming Zhu, Fangneng Zhan, Christian Theobalt, and Marc Habermann. Trihuman: a real-time and controllable triplane representation for detailed human geometry and appearance synthesis. *ACM Transactions on Graphics*, 44(1):1–17, 2024. 3
- [90] Wojciech Zielonka, Timur Bagautdinov, Shunsuke Saito, Michael Zollhöfer, Justus Thies, and Javier Romero. Drivable 3d gaussian avatars. In *International Conference on 3D Vision (3DV)*, 2025. 2, 3

RePerformer: Immersive Human-centric Volumetric Videos from Playback to Photoreal Reperformance

Supplementary Material

Within the supplementary material, we provide:

- Implementation details in Appendix Sec. A.
- Qualitative and Quantitative comparison with Animatable Gaussians [38] in Appendix Sec. B.
- Additional ablative studies in Appendix Sec. C.

A. Implementation Details

Initialization. We initialize approximately 50,000 motion Gaussians in the canonical frame using a uniform random distribution. During subsequent optimization, aside from the photometric loss in Eq. 1, the isotropic loss and size loss are defined as follows:

$$E_{\text{iso}} = \frac{1}{N} \sum_{i=1}^N \text{ReLU}(e^{\max(s_i) - \min(s_i)} - r),$$

$$E_{\text{size}} = \sum_{i=1}^N \text{ReLU} \left(s_i - \alpha \frac{1}{N} \sum_{i=1}^N sg[s_i] \right),$$
(9)

where s_i represents the scaling parameters of the i -th Gaussian, N denotes the number of Gaussians, and e is the exponential activation function. The isotropic loss ensures the ratio between the major and minor axes of each Gaussian does not exceed r (set to 4 in our experiments). The sg denotes stop-gradient operator. For appearance Gaussians, we use the initialized motion Gaussians as input and further optimize it with densification and prune as the original 3DGS [30].

Network Architecture. We use three identical U-Net architectures, adjusting the output feature dimensions to accommodate different attributes. Each U-Net incorporates a self-attention layer to maintain global consistency. As illustrated in Fig. 10, the self-attention layer is applied before the final downsampling step of the U-Net.

Re-performance. During the alignment phase, we assign semantic labels to specific regions, including the head, left hand, right hand, left foot, and right foot, to align corresponding clusters between the source and target Gaussians. For objects, we use pairwise semantic prompts (e.g., “basketball” and “balloon”) and assign consistent labels during the unprojection process, ensuring accurate alignment across different objects. The re-performance stage employs the Adam optimizer, with the alignment phase trained for 15,000 iterations and the motion transfer phase for 2,000 iterations.

Our method efficiently generates Gaussian sequences for high-fidelity playback and vivid re-performance of gen-

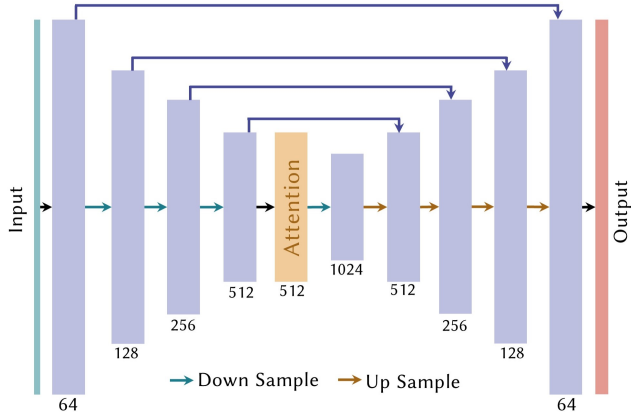


Figure 10. Network architecture.

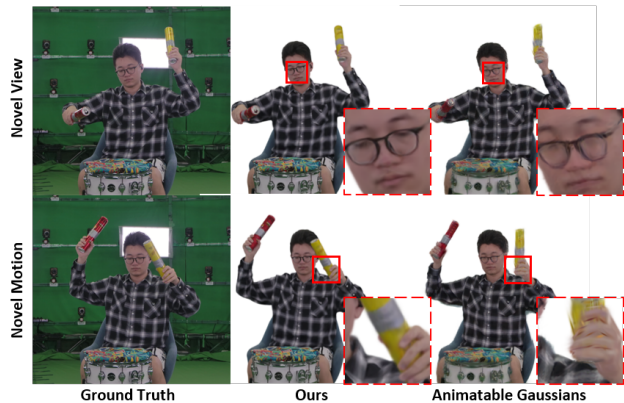


Figure 11. Qualitative comparison with Animatable Gaussians [38].

eral non-rigid scenes. We train the model using the PyTorch framework on a single NVIDIA GeForce RTX3090 GPU, achieving a rendering speed of 7 FPS. The Gaussian sequences can be further baked and compressed via DualGS [27], allowing seamless integration into low-end devices like VR headsets and iPads for intuitive, user-friendly interaction as demonstrated in Fig. 12.

B. Comparison

We further compare our method with Animatable Gaussians [38] to evaluate its rendering quality on novel views and motions. As shown in Fig. 11 and Tab. 3, this method relies heavily on the human parametric model SMPL [44], which constrains its ability to accurately estimate motion in regions far from the human body. This limitation results in severe artifacts when handling general non-rigid scenarios.

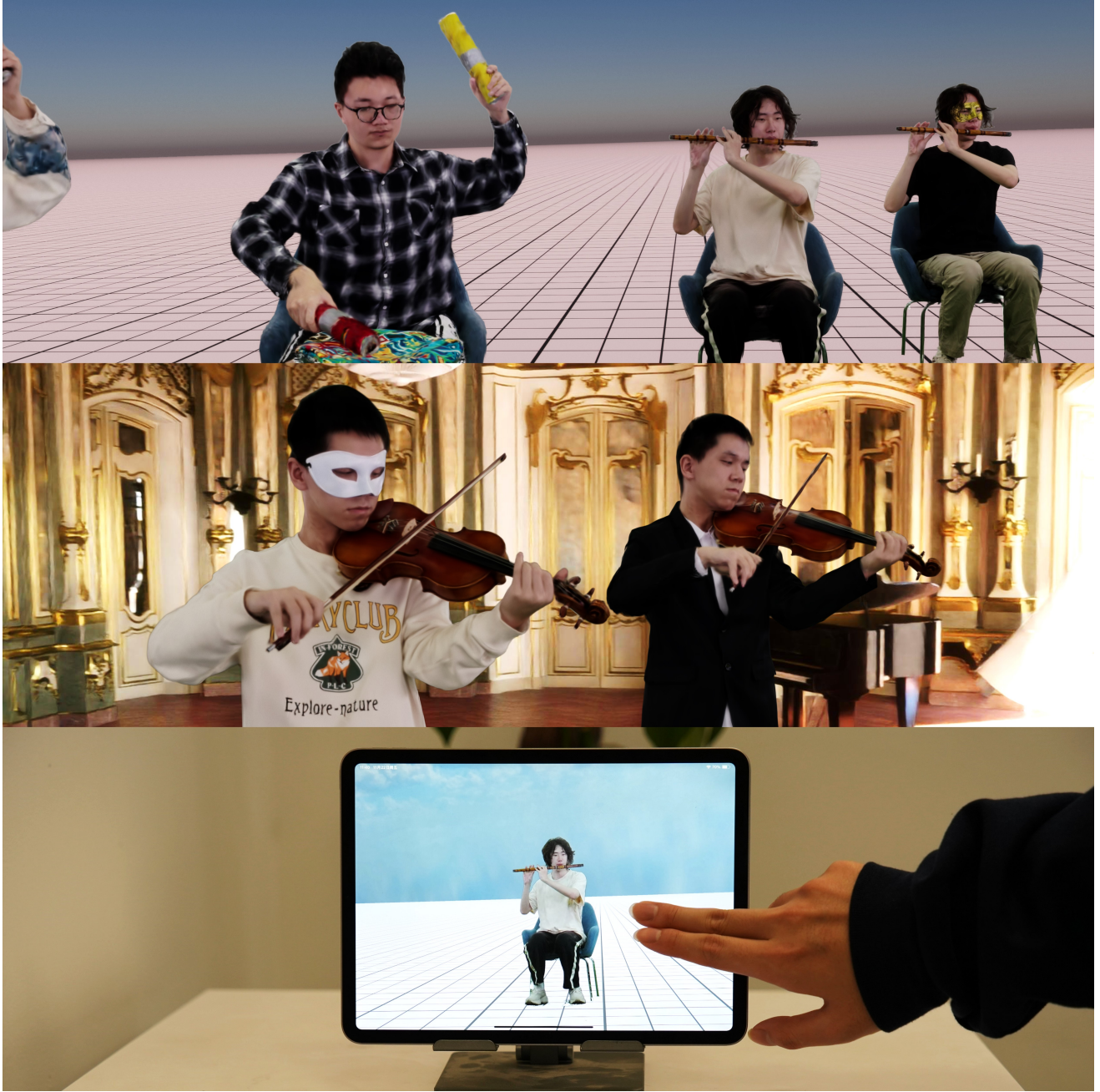


Figure 12. We further compress our Gaussian sequences using DualGS, demonstrating their adaptability in various immersive applications.

Methods	Novel View			Novel Motion		
	PSNR \uparrow	SSIM \uparrow	LPIPS \downarrow	PSNR \uparrow	SSIM \uparrow	LPIPS \downarrow
Animatable Gaussians	24.26	0.934	0.0647	22.04	0.911	0.079
Ours	32.09	0.979	0.0310	30.06	0.976	0.0277

Table 3. Quantitative comparison with Animatable Gaussians [38].

C. Ablations

Number of Camera Views. To assess the robustness of RePerformer under sparser input views, we perform ablation experiments using uniformly selected subsets of 20, 40, and 60 camera views for training, denoted as w/20.cam, w/40.cam, and w/60.cam. As shown in Tab. 4, our method maintains satisfactory rendering quality even with sparser input views.

Position Map Resolution. As illustrated in Tab. 5, we con-

Methods	PSNR \uparrow	SSIM \uparrow	LPIPS \downarrow
w/20.cam	30.36	0.971	0.0471
w/40.cam	30.89	0.975	0.0447
w/60.cam	31.33	0.977	0.0429
Ours	32.09	0.979	0.0310

Table 4. Quantitative Ablation Study on the different input view numbers.

Methods	PSNR \uparrow	SSIM \uparrow	LPIPS \downarrow
w/ 64.res	28.85	0.949	0.0887
w/ 128.res	32.82	0.981	0.0413
w/ 256.res	33.45	0.986	0.0283
w/o atten	34.16	0.990	0.0197
Ours	34.27	0.989	0.0227

Table 5. Quantitative Ablation Study on the resolution of position maps.

duct ablation studies with position map resolutions of 64, 128, 256, and 512 (ours), corresponding to different numbers of Gaussians. Although larger position maps can store denser Gaussians, they exceed GPU memory limitations. We also compare results without the self-attention layer. Our full pipeline achieves high-fidelity rendering quality at a resolution of 512 with the self-attention module, as shown in Tab. 5.